Dynamic Formation of the Protein-Lipid Pre-fusion State

Maria Bykhovskaia

Department of Neurology, Wayne State University, Detroit MI 48201

mbykhovs@med.wayne.edu

Abstract

Synaptic vesicles (SVs) release neuronal transmitters by the fusion with the presynaptic membrane (PM), and the SV protein Synaptotagmin 1 (Syt1) serves as a Ca^{2+} sensor for evoked fusion. Syt1 is thought to trigger fusion by penetrating into PM upon Ca^{2+} binding, however the mechanistic detail of this process are still debated. Syt1 interacts with the SNARE complex, a coiled-coil four-helical bundle that mediates the SV-PM attachment, and the protein Complexin (Cpx) attaches to the SNARE bundle and promotes Ca^{2+}-dependent fusion. We employed all-atom molecular dynamics (MD) to investigate the formation of the Syt1-SNARE-Cpx complex interacting with PM and SV. Our simulations demonstrated that the PM-Syt1-SNARE-Cpx complex can transition to a "dead-end" state, wherein Syt1 attaches tightly to PM but does not immerse into it, as opposed to a pre-fusion state, which has the tips of the calcium-bound C2 domains of Syt1 inserted into PM. We simulated the sequence of Syt1 conformational transitions, including Syt1 docking to the SNARE bundle and PM, as well as Ca^{2+} chelation, and found that the direct Syt1-Cpx interaction is required to promote these transitions. We developed the all-atom dynamic model of the Cpx-mediated sequence of conformational transitions that lead to the formation of the pre-fusion state of the PM-Syt1-SNARE-Cpx complex. We also show that an alternative "dead-end" complex can be formed if this pathway is disrupted.

Introduction

Neuronal transmitters are packaged in synaptic vesicles (SVs) and released by the fusion of SVs with the presynaptic membrane (PM). Action potentials trigger SV-PM fusion by inducing an inflow of Ca^{2+} into the nerve terminal, and the SV protein Synaptotagmin 1 (Syt1) serves as a Ca^{2+} sensor[3, 4] . Syt1 is a tansmembrane (TM) protein with its cytosolic region being comprised of two domains, C2A and C2B [5]. Each domain has two loops forming a Ca^{2+} binding pocket, and in each of the pockets Ca^{2+} ions are chelated by five aspartic acids [6, 7]. It is agreed that the synergistic coordinated insertion of the tips of the C2 domains into the phospholipid membrane drives fusion[3, 8, 9], but other mechanistic details of Syt1 action are still debated.

Syt1 is interacts with the SNARE complex[10-12], a coil-coiled four-stranded helical bundle made up of the PM-associated proteins (also known as t-SNARE) syntaxin-1A (Sx) and SNAP25, as well as the SV protein synaptobrevin (Sb) or v-SNARE. The SNARE complex mediates the SV-PM attachment, and the SNARE assembly overcomes the electrostatic and hydration repulsion between the lipid bilayers [13]. Multiple studies suggest an important role for the Syt1-SNARE interactions [1, 14-18], however it is still debated how the Syt1-SNARE complex is formed *in vivo*.

A cytosolic protein Complexin (Cpx) attaches to the SNARE bundle[19] and serves as a positive regulator of synchronous release, promoting and accelerating evoked synaptic transmission[20-25] . The effect of Cpx on synchronous fusion is Ca^{2+}-dependent [20] and several studies suggested a functional [25-29] or molecular [30] interaction between Cpx and Syt1. However, it is still debated how Cpx promotes and synchronizes evoked transmission.

The Syt1-SNARE complex adopts multiple conformational states[1, 18, 30-32] , and it is still obscure how the complex is formed between the lipid bilayers of SV and PM. The molecular dynamics

(MD) approach proved to be instrumental in addressing this problem [33, 34], however, the simulation time-scales represent a critical limitation of MD since the conformational transitions of Syt1 occur at a scale of microseconds[35]. Therefore, we took advantage of Anton2 supercomputer customized for MD [36, 37], which enables the simulations of protein-lipid complexes at the time-scales of microseconds and up a sub-millisecond range [38, 39]. We have recently employed this approach to build the all-atom model of the PM-Syt1-SNARE-Cpx complex[2]. The present study investigates the conformational pathway of the complex to its prefusion state.

Results

The PM-Syt1-SNARE-Cpx complex can adopt the "dead-end" state, which has Syt1 tightly attached to PM but not penetrating into the lipid bilayer

The primary interface between t-SNARE and the C2B of Syt1 (strands β1, β2, β5, and β8) has identified crystallography[1]. A subsequent *in vivo* study in *Drosophila* revealed multiple loss-of-function mutations in Syt1 pertaining to this interface[17], and MD simulations revealed that its formation promotes the immersion of the tips of the C2 domains into PM and drives the SV-PM fusion [2]. However, multiple conformational states of the Syt1-SNARE complex have been detected *in vitro*[18, 31] and *in silico*[2], raising the question of whether some of these states can serve as intermediates in the formation of the pre-fusion protein-lipid complex. To elucidate these question, we employed the MD approach to test two scenarios: 1) Syt1 anchors to the SNARE bundle via the primary interface; and 2) Syt1 anchors to the SNARE bundle forming an intermediate state, and undergoes conformational transition(s) leading to the pre-fusion state.

As a starting point, we took the Syt1-SNARE-Cpx complex obtained by crystallography [1] followed by MD [2], which had the C2B domain attached to t-SNARE via its primary interface. The protein complex

was the positioned onto the lipid bilayer mimicking PM (Fig. 1 A), so that the PM-binding motifs of Syt1, including is polybasic (PB) regions [40, 41] contacted PM. A subsequent MD run (4.8 μs, Video 1, Fig. 1 B) produced a conformational transition within the initial 2 μs, so that the C2A domain separated from the SNARE bundle, attached to its N-terminus (Fig. 1 C, Transitional state) and then attached to PM (Fig. 1 B, Final state). Subsequent 3 μs of the simulations (Fig. 1 B) did not produce any further alterations: both C2 domains remained attached to PM with their Ca^{2+}-binding loops (CBLs) facing each other (Fig. 1 C, Final state; D). The attachment of both C2 domains to PM was mediated by the salt bridges with phosphotidylinositon 4,5-biphosphate (PIP_2) monomers (Fig. 1 B, black). The C2B-SNARE interface remained intact, being largely maintained by the salt bridges between R281 of Syt1 and E51/E55 of SNAP25, as well as between E295 of Syt1 and K40 of SNAP25 (Fig. 1 D, E).

Next, we investigated how Syt1 would bind Ca^{2+} within the obtained PM-Syt1-SNARE-Cpx complex. Ca^{2+} chelation was simulated employing the method of K^+/Ca^{2+} replacement[35]. We examined all the time-points of the final 250 ns stretch of the MD trajectory (presented in Fig. 1), which had K^+ ions inside the Ca^{2+} binding pockets of both C2 domains. We then selected three time-points which had three K^+ ions inserted between the CBLs of the C2A domain[6] and two K^+ ions inserted between the CBLs of the C2B domain [42]. We next replaced the five K^+ ions by Ca^{2+} and generated three 6.8 μs MD runs starting from the three initial states described above.

Strikingly, all the three MD runs produced the complexes with Ca^{2+} ions bridging the CBLs of the C2A and C2B domains (Fig. 2). In each run, one or two Ca^{2+} ions dissociated from Syt1, leaving three or four Ca^{2+} ions chelated by Syt1. The first run had four Ca^{2+} ions chelated (Fig. 2 A, B; note one of the ions having zero interaction energy with Syt1, ochre). In this run, two Ca^{2+} ions were bridging the C2A and C2B domains, while each of the other two Ca^{2+} ions was chelated by either C2A or C2B domain only (Fig. 2 A, C). The other two runs (Run 2 and 3) had three Ca^{2+} ions remaining chelated in the end of the trajectory, with one of the chelated Ca^{2+} ions bringing the CBLs of C2A and C2B domains (Fig. 2 C).

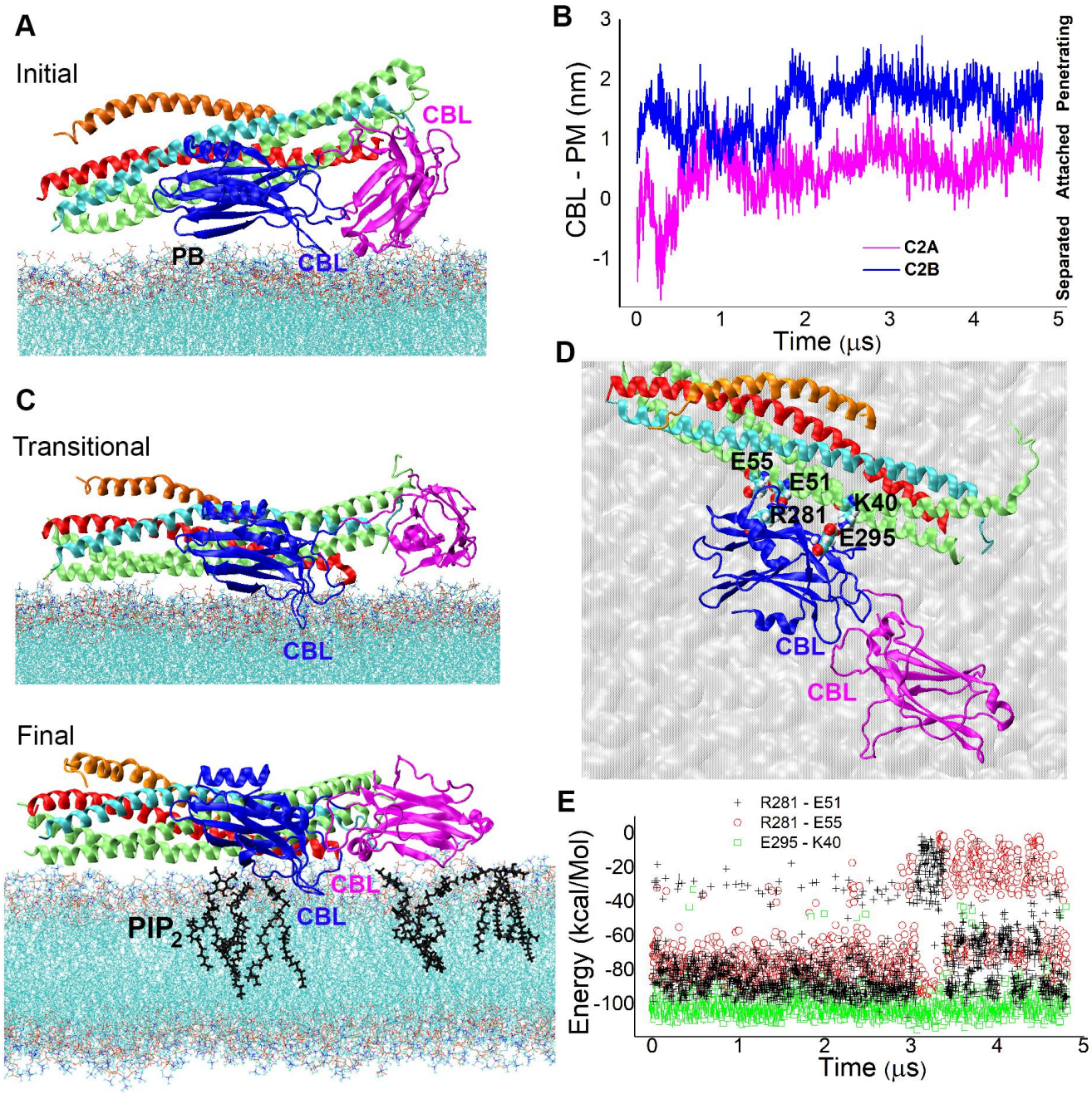

Fig. 1. The attachment of Syt1 to the SNARE-Cpx complex via the primary interface produces the PM-Syt1-SNARE-Cpx complex with the CBLs of the C2 domains facing each other. **A.** The Syt1-SNARE-Cpx complex with the C2B domain attached to t-SNARE via the primary interface[1, 2] is positioned onto PM in such a way that the PB stretches are touching PM. Magenta: C2A domain; blue: C2B domain; red: Sb; cyan: Sx; lime: SNAP25; orange: Cpx. **B.** The C2A domain undergoes a conformational transition (arrow) and then attaches to PM. **C.** The transitional and final states of the PM-Syt1-SNARE-Cpx complex. Note that the final state has both domains anchored to PM via interactions with PIP_2, **D.** The top view of the final PM-Syt1-SNARE-Cpx complex showing the primary C2B-SNARE interface maintained by the salt bridges: R281(Syt1)-E55(SNAP25); R281(Syt1)-E51(SNAP25); E295(Syt1)-K40(SNAP25). Note the CBLs of the C2 domains facing each other. **E.** One of the salt bridges (green) remains continuously stable along the trajectory, while the other salt bridges either alternate (in the second half of the trajectory) or form simultaneously.

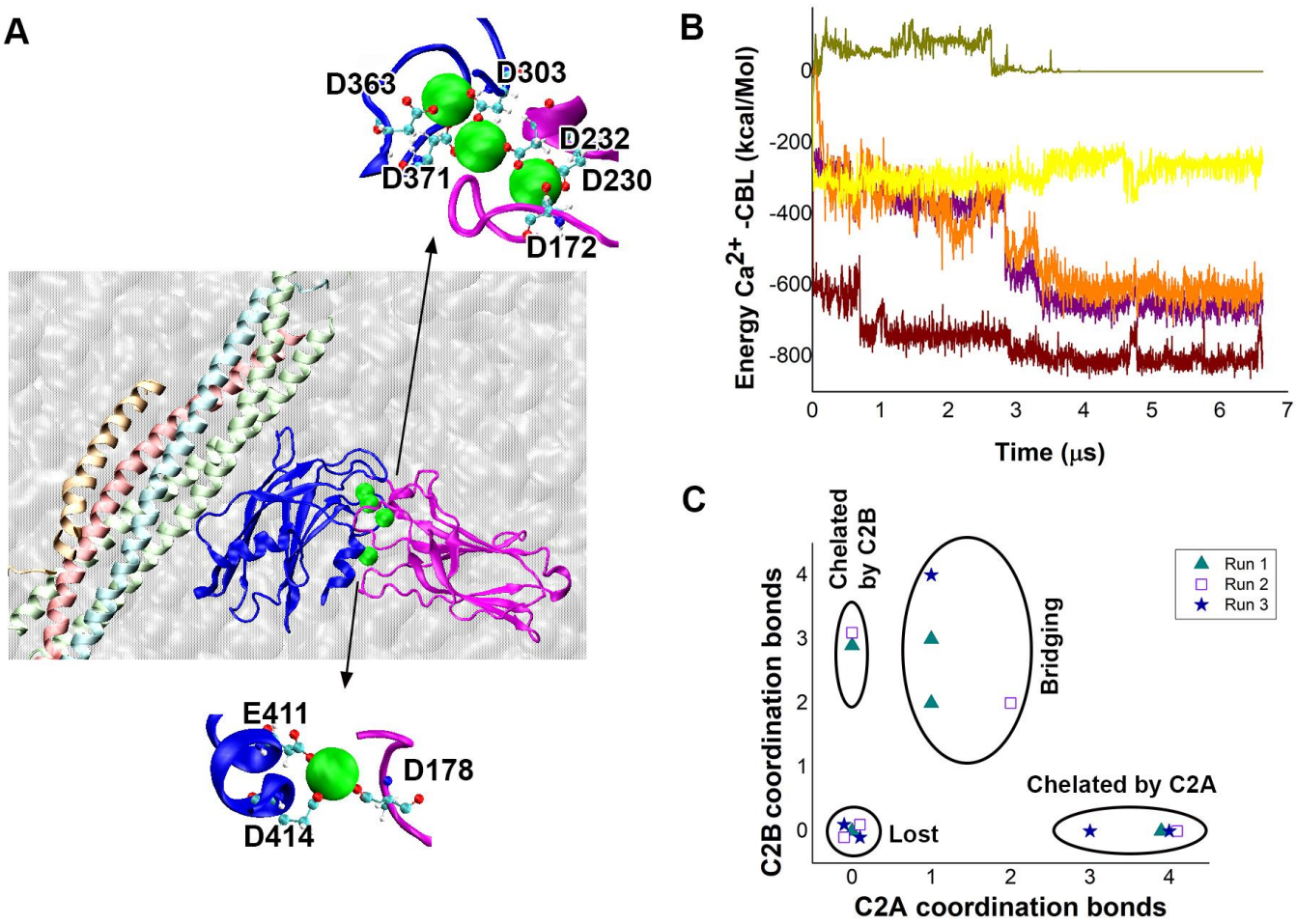

Fig. 2. The Ca^{2+} ions chelated within the PM-Syt1-SNARE-Cpx complex bridge the CBLs of the C2A and C2B domains. **A.** The PM-4Ca^{2+}Syt1-SNARE-Cpx complex in the end of the Run 1. Four ions (green spheres) are chelated. One of the Ca^{2+} ions is bridging the CBLs of the C2 domains (D303, D371, D232) while another Ca^{2+} ion is bridging the CBL of the C2A domain (D178) with the C-terminus of the C2B domain (E411 and E414). **B.** The energy of the interactions of the five Ca^{2+} ions (marked by different colors) with the CBLs of Syt1 over the course of the Run 1. Note that one of the ions (ochre) is "lost" after the initial 3 μs, as the interaction energy approaches zero. The remaining four Ca^{2+} ions formed stable coordination bonds. **C.** The results of the three MD runs. Each data point corresponds to a single Ca^{2+} ion in the end of the trajectory. Note that each run produced bridging of the C2A-C2B domains by either one (Runs 2 and 3) or two (Run 1) Ca^{2+} ions.

These results show that if Ca^{2+} ions are chelated after the C2A and C2B domains of Syt1 attach to PM, the Ca^{2+} coordination can be drastically altered. Indeed, it was demonstrated *in vitro*[1] and *in silico*[35] that when phospholipid bilayers are not present, the Syt1 dimer, isolated or within the Syt1-SNARE complex,

chelates four Ca^{2+} ions, two by the CBLs of each domain, and no bridging between the C2 domains takes place.

We next investigated how the formation of the bridged PM-4Ca^{2+}Syt1-SNARE-Cpx complex would affect the ability of the C2 domains of Syt1 to insert into PM. The Run 1 was continued for additional 7.2 μs, and the penetration of the C2 domains into PM over the course trajectory was analyzed (Fig. 3 A). We found that the penetration of the CBLs of the C2 domains did not increase over the course of the trajectory, and for the C2B domain it even slightly diminished (Fig. 3 A, blue), suggesting that bridging of the CBLs counteracts their immersion into the lipid bilayer. Indeed, in the end of the trajectory, both C2 domains were tightly attached to PM but not inserted into it (Fig. 3 B, C2 domains bridged).

Notably, this finding sharply contrasts the results of the earlier MD study[2] , obtained for the PM-4CA^{2+}Syt1-SNARE-Cpx complex with the uncoupled domains (Fig. 3 B, C2 domains uncoupled).

The latter complex was generated by positioning the 4Ca^{2+}Syt1-SNARE-Cpx complex onto PM, which was followed by a prolonged MD run[2]. Together, these results suggest that the PM-4Ca^{2+}Syt1-SNARE-Cpx complex can be formed via different pathways, and that these pathways can determine the level of the insertion of the C2 domains of Syt1 into PM. Indeed, the results presented in figure 3 show that the Ca^{2+} bound tips of the C2 domains would insert into PM if the Ca^{2+} ions are chelated prior to the attachment of Syt1 to PM, while the C2 domains they would not insert into PM if the Ca^{2+} chelation follows the attachment Syt1 to PM (Fig. 3 C).

We questioned therefore what is the sequence of events and interactions of Syt1 that leads to the formation of the pre-fusion PM-4Ca^{2+}Syt1-SNARE-Cpx complex that enables the C2 domains of Syt1 to insert into PM and to drive fusion.

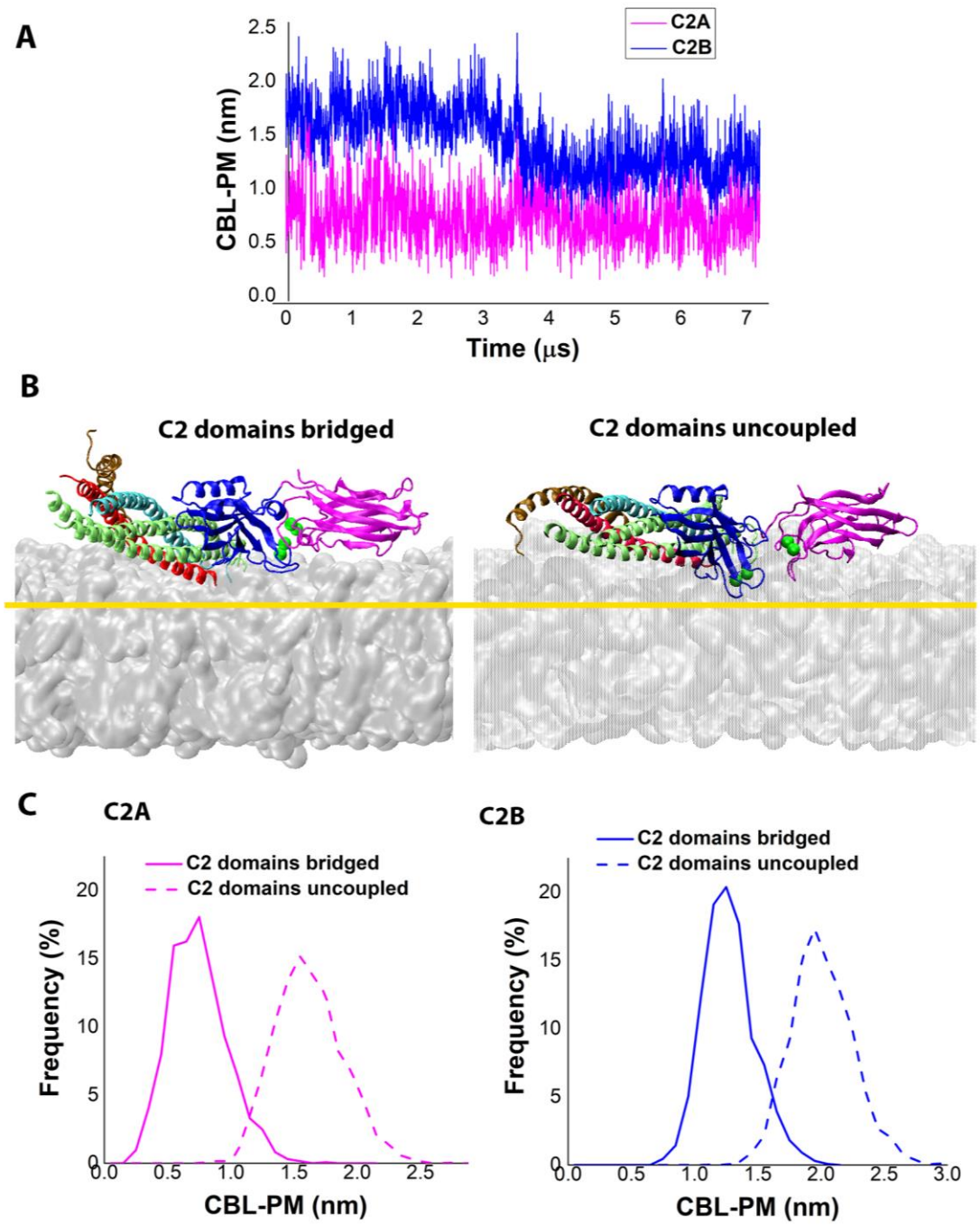

Fig. 3. The comparison of the PM-4Ca^{2+}Syt1-SNARE-Cpx complexes with bridged and uncoupled C2 domains. **A.** The bridged PM-4Ca^{2+}Syt1-SNARE-Cpx shows no penetration into PM over the course of the trajectory Note the steady C2A-PM attachment (magenta) and diminishing C2B-PM penetration (blue). **B.** The bridged (this study) versus uncoupled [2] complexes in the end of respective trajectories. The yellow line denotes the penetration into PM for the complex with the uncoupled C2 domains. **C.** The complex with the bridged C2 domains has a significantly lower level of the penetration into PM ($p<0.001$ per K-S test) compared to the complex with the uncoupled C2 domains (data replotted from[2]).

Syt1 docks to the SNARE bundle via the association of the C2B domain with SNAP25 and PM, and subsequently the PM-Syt1-SNARE-Cpx complex transitions to an intermediate state with the C2A domain of Syt1 being attached to Cpx

We started from simulating the dynamics of the full-length Syt1 attached to SV. The initial 3D structure of the human full-length Syt1, ($Syt1^{fl}$, Fig. 4 A) was generated employing homology modeling as described in Methods. The TM domain (TMD) of $Syt1^{fl}$ was then inserted in the lipid bilayer mimicking SV, and all the lipid monomers overlapping with the TMD of Syt1 were removed (Fig. 4 B). Following the equilibration of the system, a 3.6 μs MD run was performed. The TMD of Syt1 retained its helical structure over the entire length of the trajectory, remaining inserted into the lipid bilayer. The orientation of the C2A domain remained largely the same over the entire course of the trajectory (Fig. 4 C, D), with its CBLs being in the proximity to the lipid bilayer but usually not attached to it, being separated from the bilayer by the linker domain connecting TMD with the C2A domain. The linker was largely unstructured, with the exception of a short alpha helix formed by the residues 107-118 (DVKDLGKTMKDN), which was stable over the entire length of the trajectory (Fig. 4 D, black). The linker helix interacted with the lipid bilayer and with the C2A domain, being often positioned between the two (Fig. 4 D: points 1, 3, 4, 5). Notably, the C2B domain was highly mobile (Fig. 4 C-E), being typically distanced from the lipuid bilayer Fig. 4 D: points 1, 3, 4, 5, 6, 7), but sometimes attaching to it (Fig. 4 D: points 2, 8).

The observed mobility of the C2B domain and its distancing from the SV bilayer could be favorable for anchoring to the SNARE bundle or PM, or possibly both. To investigate whether this is the case, we added the SNARE-Cpx complex to the system. The SNARE-Cpx bundle was oriented parallel to the lipid bilayer, and Z-dimension was adjusted so that the C2B domain would approach the leaflet mimicking PM (Fig. 5 A.1). The SNAP25 helixes and the C2B domain were in a proximity but did not interact (Fig. 5 A.2). The system was then equilibrated and a 7 μs MD run was performed.

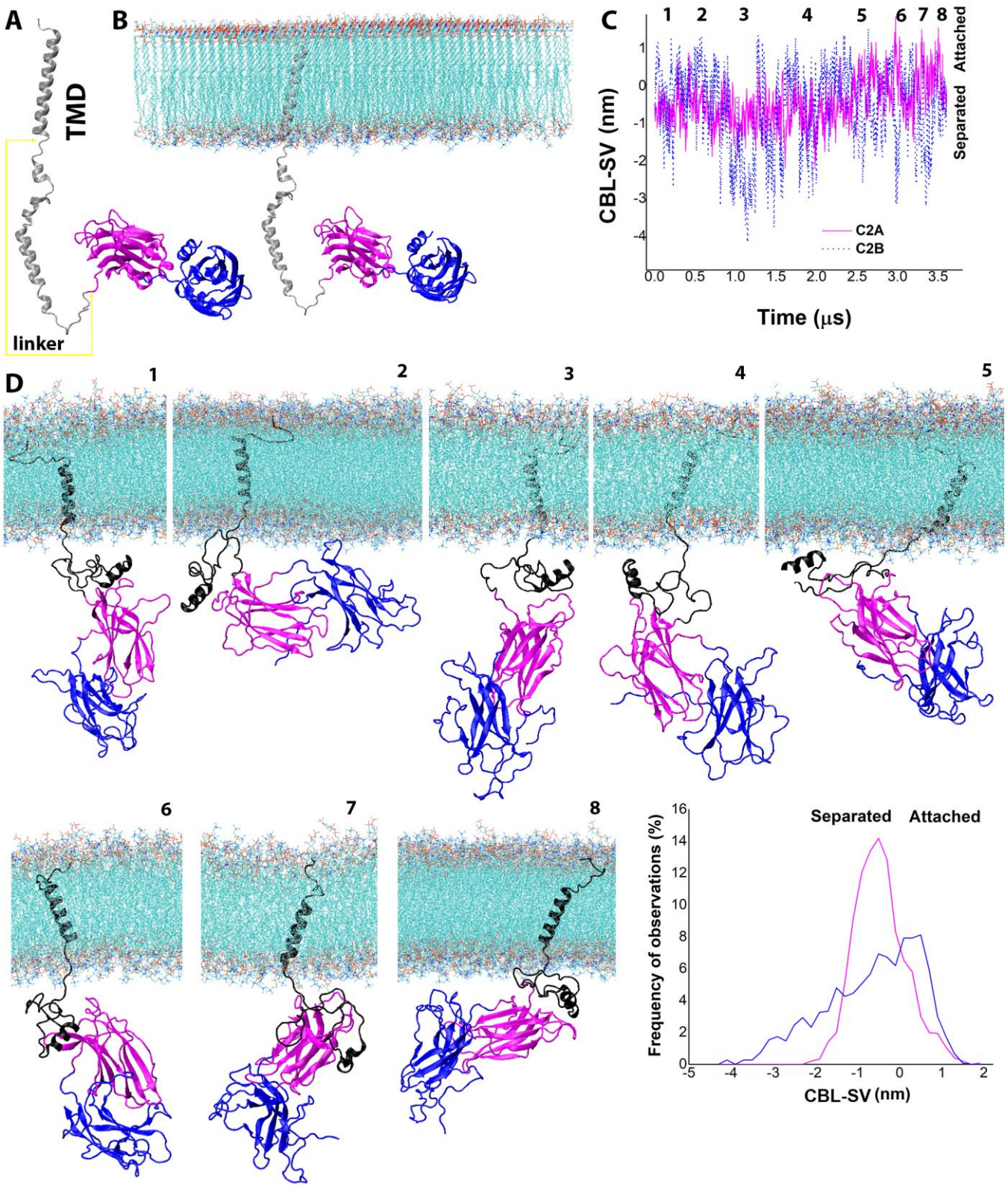

Fig. 4. The dynamics of Syt1^{fl} attached to the lipid bilayer mimicking SV. **A.** The initial Syt1^{fl} structure with the linker domain and TMD. **B.** TMD inserted in the lipid bilayer. **C.** The attachment/separation of the CBLs of the C2 domains to/from the SV lipid bilayer. The time-points 1-8 correspond to the states shown in the panel D. **D.** The states of Syt1^{fl}-SV complex along the trajectory. **E.** The frequency distributions for the CBL-SV separation/attachment. Note that the C2A domain (magenta) predominantly remains in the SV proximity, while the C2B domain (blue) alternates between distancing and attachment.

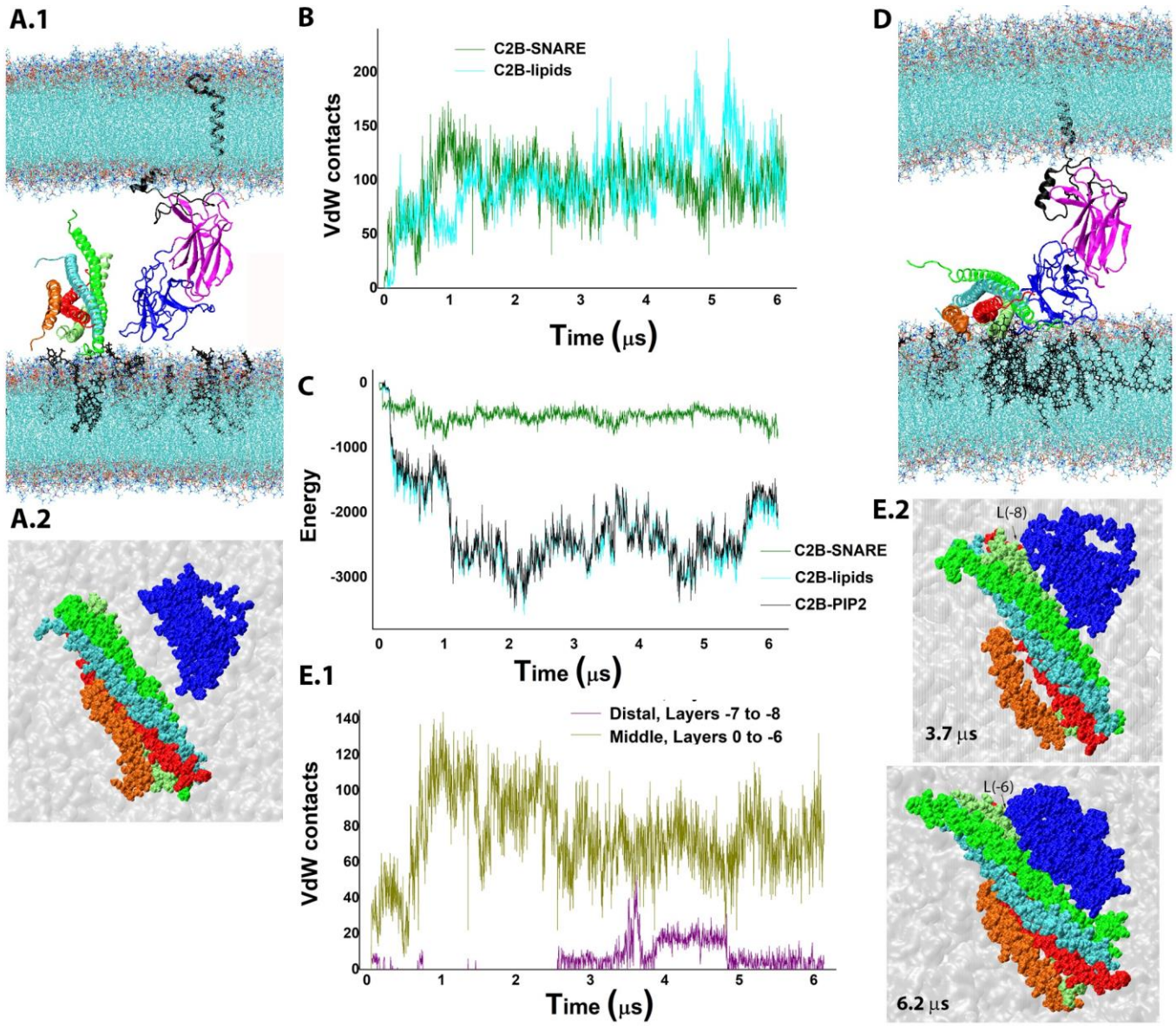

Fig. 5. The C2B domain of the SV-attached Syt1^{fl} anchors simultaneously to t-SNARE and to PIP_2. **A.** The initial state of the molecular system. **A.1** The SNARE-Cpx bundle is positioned in the vicinity of the C2B domain (blue) and parallel to the lipid bilayer, with SNAP25 (green) facing Syt1. The height of the cell is adjusted so that the C2B domain is touching the PM bilayer, which incorporates PIP_2 (black). **A.2.** The top view of the SNARE-Cpx bundle and the C2B domain on PM in the VdW representation. The rest C2A domain, linker and TMD of Syt1 are removed for clarity. **B.** The number of contacts between the C2B domain and the SNARE bundle rapidly increases, followed by the increase in the number of contacts between the C2B domain lipids. **C.** The energy of the interactions between the C2B domain and lipids dominates over the energy of the C2B-SNARE interactions, and the former is largely defined by the C2B-PIP_2 interactions. **D.** The final state of the system in the end of the trajectory: the C2B domain is docked tightly to SNAP25 and attached to the PIP_2 cluster (black). **E.** The C2B domain shifts from the middle of the bundle to its distal end (N-terminus) and back over the simulation trajectory. **E.1** The $\beta_1\beta_2$ $\beta_5\beta_8$ surface of C2B domain forms transient contacts with the distal layers of the bundle (L(-7) and L(-8)) in the middle of the trajectory (purple) and remains in contact with the middle of the bundle (ochre) over the entire length of the simulation. **E.2.** The states with the C2B domain shifted towards the distal end of the bundle (top) and towards the middle of the bundle (bottom).

We observed a rapid docking of the $\beta_1\beta_2$ $\beta_5\beta_8$ surface of the C2B domain to SNAP25 (Fig. 5 B, C, green, D). This was accompanied by and a slower attachment of the polybasic stretch of the C2B domain to the lipid bilayer mimicking PM (Fig. 5 B, C, cyan, D). The energy of the C2B-lipid interactions was largely defined by the C2B-PIP_2 component (Fig. C, black), and it dominated over the C2B-SNARE interactions (Fig. 5 C, cyan versus green). This result indicates that the C2B-PM interactions driven by the strong electrostatic attachment of the PB stretch of the C2B domain to PIP_2 would dominate and largely determine the configuration and dynamics of the Syt1-SNARE docking.

Interestingly, we observed the movement of the C2B module along the SNARE bundle over the course of the trajectory (Fig. 5 E). Initially, the C2B module was attached between the ionic layer in the middle of the bundle and the layer L(-6) at the N-terminal (distal) end of the bundle (Fig. 5 E.1, ochre). Subsequently, the C2B domain shifted to the distal end of the bundle to the layer L(-8) (Fig. 5 E.1, purple; Fig. 5 E.2, 3.7 μs) and then shifted back more proximally (Fig. 5 E.2, 6.2 μs). This transitions are in line with the earlier finding that the Syt1-SNARE complex can adopt multiple conformational states [31].

It should be noted, however, that our system (Fig. 5) had extra degrees of freedom, since the SNARE bundle was not attached to PM via the TM domain of Sx. Therefore, we sought to investigate the dynamics of the PM-Syt1-SNARE-Cpx complex under more realistic conditions, with the TM domain of Sx being included and inserted in PM.

We substituted Sx within the obtained PM-Syt1-SNARE-Cpx complex (shown in Fig. 5 D) by Sx^{TM} , which included the TM domain of Sx. The model of Sx^{TM} with the bent TM domain was generated in our earlier MD study[2], As described in [2], we replaced the zippered domain of Sx within the PM-Syt1-SNARE-Cpx complex by Sx^{TM} . Subsequently, the TM domain of Sx^{TM} was inserted into the lipid bilayer mimicking PM, and the lipid monomers interfering with the TM domain were manually removed. Finally,

we removed from the system the TM of Syt1 together with the linker. This was needed to avoid the artificial coupling of the TM domains of Sx and Syt1 via the lipid bilayer and its periodic image.

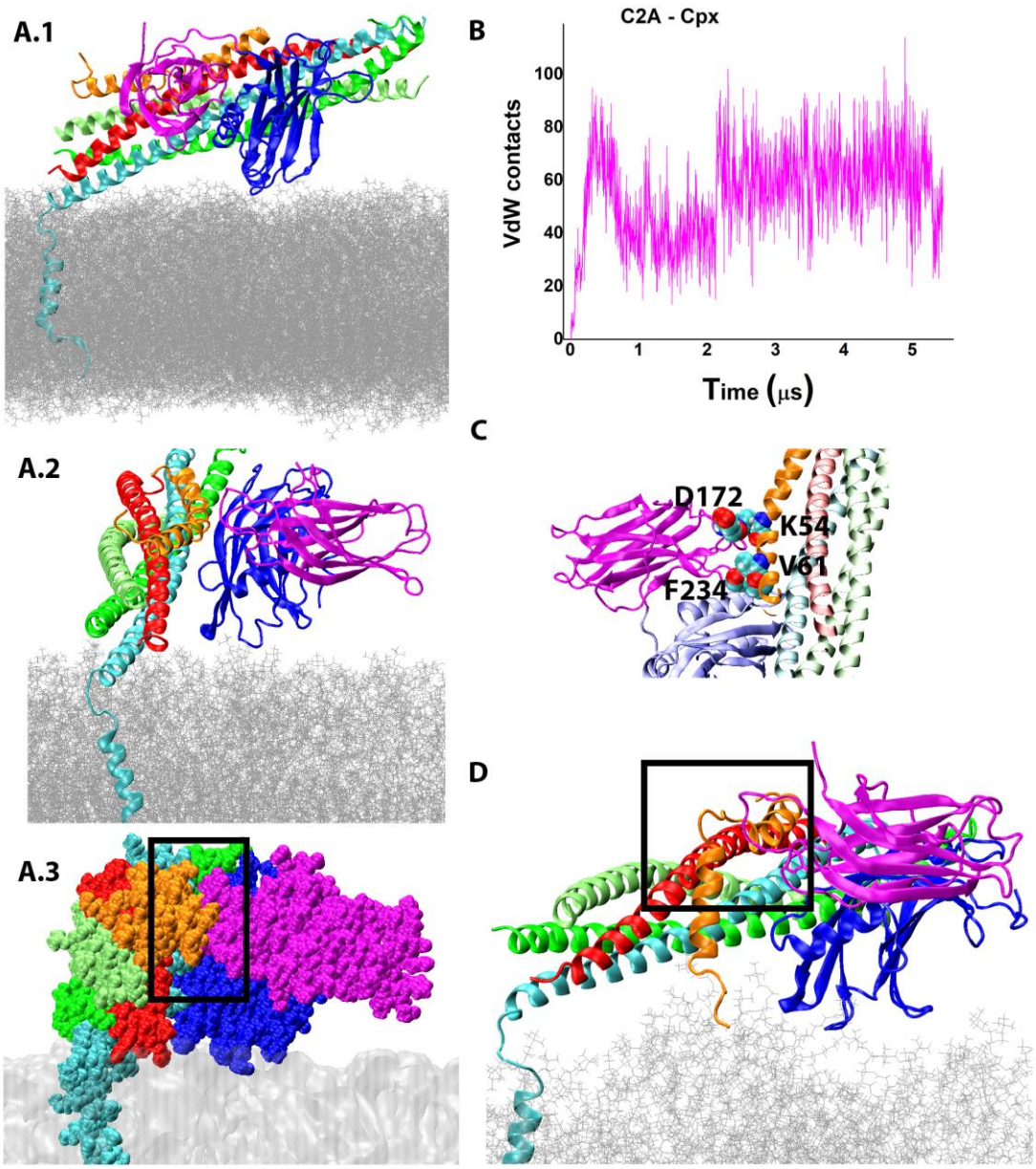

Fig. 6. The C2A-Cpx attachment within the PM-Syt-SNARE^{TM}-Cpx complex. **A.** Three views of the complex showing the interactions of the CBLs of the C2A domain of Syt1 (magenta) with the SNARE-attached Cpx (orange). The two perpendicular views in cartoon representation (A.1 and A.2) show the C2B domain (blue) attached to SNAP25 (green) in the middle of the SNARE bundle and the C2A domain in contact with Cpx. Note the TM domain of Sx1A^{TM} (cyan) inserted into PM (silver). The VdW representation (A.3) shows the tight contacts between the CBLs of the C2A domain and Cpx (boxed). **B.** The C2A-Cpx attachment is formed within the initial 300 ns of the simulations and remains intact over the entire course of the 5.6 μs trajectory. **C.** The C2A domain of Syt1 forms a salt bridge (D172-K54) with Cpx, which is strengthened by the hydrophobic interactions (F234-V61). **D**. A kink between the Cpx central and accessory helixes appear in the end of the trajectory, displacing the accessory helix of Cpx from the SNARE bundle.

The system was then equilibrated, and the 5.6 µs MD run of the PM-Syt1-SNARE^{TM}-Cpx complex was performed (Fig. 6). Within the initial 300 ns of the simulation, tight contacts were formed between the CBLs of the C2A domain and the region of Cpx (Fig. 6 A, B). The C2A-Cpx attachment (Fig. 6 C) was largely maintained by a salt bridge (D172 of Syt1 – K54 of Cpx) and by strong hydrophobic interactions (F234 of Syt1 – V61 of Cpx), and it remained intact until the end of the 5.6 µs trajectory (Fig. 6 B).

Over the course of the trajectory, a kink between the Cpx central and accessory helixes developed, becoming prominent in the end of the trajectory (Fig. 6 D). This result suggests that the Syt1-Cpx interactions within the PM-Syt-SNARE^{TM}-Cpx complex may affect the Cpx conformation, displacing the Cpx accessory helix from the SNARE bundle.

Thus, our simulations revealed a new conformational state of the PM-Syt1-SNARE^{TM}-Cpx complex, which had the CBLs of the C2A domain attached to Cpx in the region connecting the Cpx central and accessory helixes (Fig. 6). Furthermore, our simulations suggest the SV-attached Syt1 and the PM-attached SNARE-Cpx bundle will likely form this complex when SV and PM are brought into proximity.

The intermediate PM-Syt1-SNARE^{TM}-Cpx complex orchestrates the sequential Ca^{2+} chelation by the C2B and C2A domains, leading to the formation of the pre-fusion state with both C2 domain of Syt1 inserted into PM

Next, we investigated how Syt1 would bind Ca^{2+} ions within the generated PM-Syt1-SNARE^{TM}-Cpx complex (Fig. 6 C). Notably, we found that the Ca^{2+}-binding pocket of the C2A domain within this complex was shielded by Cpx (Fig. 7 A.1), and therefore only the CBLs of the C2B domain ware capable of chelating Ca^{2+} (7 A.2).

We then simulated Ca^{2+} binding by the C2B domain employing the method of K+/Ca^{2+} replacement[35] as described above. Two Ca^{2+} ions were chelated within the Ca^{2+}-binding pocket (Fig. 7 B), matching the Ca^{2+} coordination obtained in earlier experimental[42] and computational [35] studies.

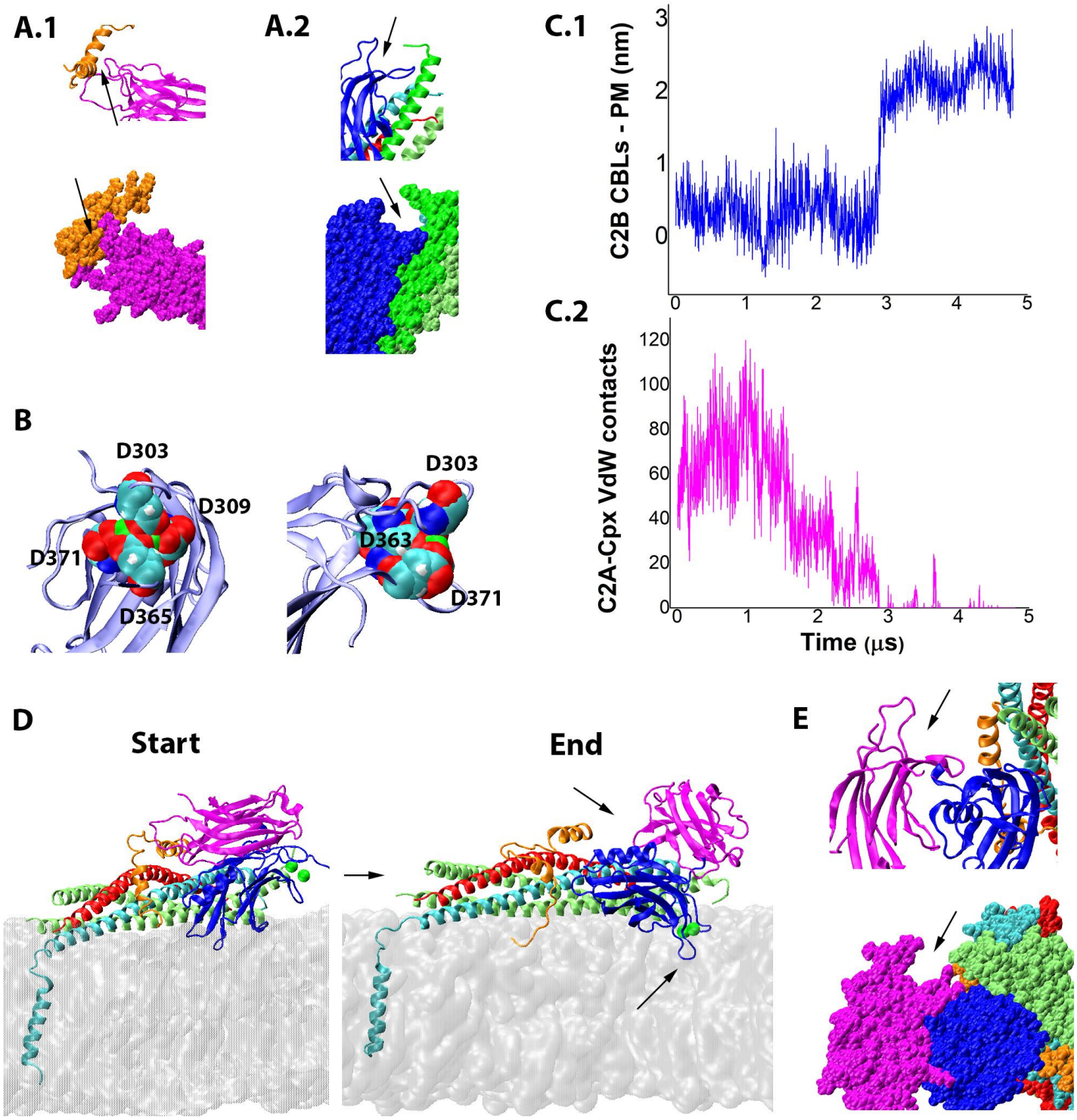

Fig. 7. Ca^{2+} binding by the C2B domain induces a conformational transition of the PM-2Ca^{2+}Syt1-SNARE™-Cpx complex, so that the tip of the C2B domain penetrates into PM and the C2A domain separates from Cpx. A. The CBLs of the C2A domains are shielded by Cpx (arrows, A.1, the SNARE bundle is removed for clarity), while the CBLs of the C2B domain are accessible (arrows, A.2). **B.** Two VdW views of the CBLs of the C2B domains with two chelated Ca^{2+} ions (green). **C.** The trajectory shows a conformational transition around 3 μs, which has the CBLs of the C2B domain penetrating into PM (C.1) and the C2A domain separating from Cpx (C.2). **D.** The initial and final states of the PM-2Ca^{2+}Syt1-SNARE™-Cpx complex. Note the CBLs of the C2A domain detached from Cpx and the CBLs of the C2B domain immersed into PM (arrows). **E.** Final state of the PM-2Ca^{2+}Syt1-SNARE™-Cpx complex has the Ca^{2+}-binding pocket of the C2A domain being open (arrow). The same view is shown in cartoon (top) and VdW representations (bottom).

Next, we performed a 4.8 MD run of the obtained PM-2Ca^{2+}Syt1-SNARE™-Cpx complex with two Ca^{2+} ions being chelated within the Ca^{2+} binding pocket of the C2B domain (Fig. 7 C). Following the initial 3 μs of the simulations, we observed a rapid conformational transition, with the CBLs of the C2B domain immersing into PM (Fig. 7 C.1, D). This was accompanied by a disruption of the C2A-Cpx attachment (Fig. 7 C.2, D, Video 3). Notably, the final state of the PM-2Ca^{2+}Syt1-SNARE™-Cpx complex had the CBLs of the C2A domain open (Fig. 7 D, E,) due to the separation of the C2A domain from Cpx.

This result suggests that the Syt1-Cpx interactions define the pattern of the Ca^{2+} chelation by the C2 domains of Syt1, so that two Ca^{2+} ions are initially bound by the C2B domain, while the C2A domain chelates Ca^{2+} upon a subsequent conformational transition. To test this hypothesis further, we simulated the Ca^{2+} chelation by the C2A domain within the obtained PM-2Ca^{2+}Syt1-SNARE™-Cpx.

Although three Ca^{2+} ions[6] were initially inserted in the Ca^{2+}-binding pocket of the C2A domain, only two ions remained chelated (Fig. 8 A), while the third Ca^{2+} ion was rapidly lost from the pocket. This finding is in line with earlier experimental[43, 44] and computational[35] studies, which suggested that the C2AB tandem can only chelate four Ca^{2+} ions, two within each C2 domain. The two chelated Ca^{2+} ions remained within the CBLs of the C2A domain over the entire length of the trajectory, forming coordination bonds with five aspartic acids (Fig. 8 A).

To investigate the dynamic behavior of the obtained PM-4Ca^{2+}Syt1-SNARE™-Cpx complex, we performed a prolonged (26.5 μs) MD run (Fig. 8, B, C). The initial 12 μs of the trajectory were characterized a relative stability of the complex, with the C2A domain remaining separated from PM (Fig. 8B; Fig. 8 D, Start), although a transient shift of the C2B domain along the bundle (Fig. 8 C) was observed. Subsequently, a conformational transition took place (Fig. 8 B, arrows), so that the C2A domain moved and rotated with its CBLs attaching to PM (Video 4). This was accompanied by a brief detachment of the C2B domain from the SNARE complex (Fig. 8C, arrows) and a subsequent shift of the C2B domain towards the proximal end of the bundle (Fig. 8C, note the lack of interactions with the distal layers in the end of the trajectory).

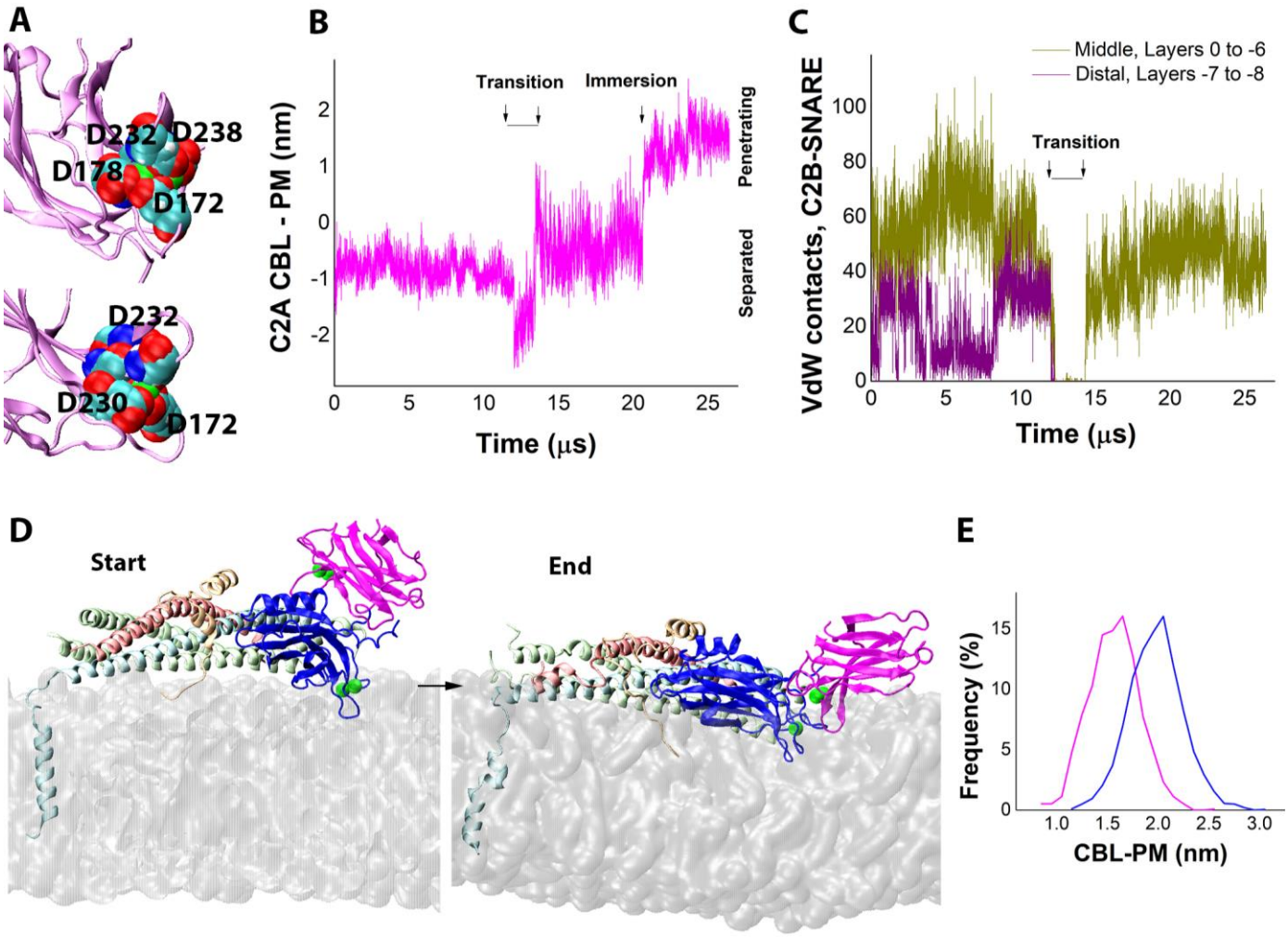

Fig. 8. The PM-4Ca^{2+}Syt1-SNARE^{TM}-Cpx complex transitions to its pre-fusion state with the tips of both C2 domains penetrating into PM. **A.** The CBLs of the C2A domain chelate two Ca^{2+} ions, which from coordination bonds with five aspartic acids. Two perpendicular views are shown. **B.** The CBLs of the C2A domain are initially separated from PM, however Syt1 undergoes a conformational transition, so that the CBLs of the C2A domain approach PM and subsequently immerse in it. **C.** The C2B domain shifts along the bundle, interacting with its distal layers in the beginning of the trajectory, but attaching to the middle of the bundle after the conformational transition. **D.** The initial and final states of the trajectory. Note that in the end of the trajectory the CBLs of both domains with chelated Ca^{2+} ions (green) penetrate into PM. **E**. The levels of the immersion of the C2 domains into PM. The frequency distributions were constructed for the final 1.5 μs of the trajectory.

Subsequently, following 21 μs of the simulations, the CBLs of the C2A domain immersed into the bilayer mimicking PM (Fig. 8 B, arrow). The end-point of the trajectory had the CBLs of both C2 domains being inserted into PM (Fig. 8 D, End; E).

Thus, our MD simulations produced the dynamic model for the formation (Fig. 5-8) of the prefusion PM-4Ca^{2+}Syt1-SNARE™-Cpx complex (Fig. 8D, End). Furthermore, the simulations suggested that this pathway is guided by a direct interaction between Syt1 and Cpx on the SNARE bundle (Fig. 6). Importantly, this pathway produced the pre-fusion state with both tips of the C2 domains inserted into PM, in contrast to the "dead-end" state of the complex (Fig. 3)

Discussion

We employed MD simulations to elucidate the conformational pathway that leads to the formation of the pre-fusion protein-lipid complex (Fig. 9). Our results suggest that the C2B domain of Syt1 (Fig. 9 (1)) docks to SNAP25 via its $\beta_1\beta_2$ $\beta_5\beta_8$ surface and almost simultaneously attaches to PM via the formation of salt bridges between the PB stretch and PIP_2 (Fig. 9 (2)). Subsequently, the CBLs of the C2A domain of Syt1 bind Cpx via strong ionic and hydrophobic interactions, and the complex transitions to an intermediate state (Fig. 9 (3)). This intermediate state allows the Ca^{2+} chelation by the C2B domain but not by the C2A domain. When the CBLs of the C2B domain bind Ca^{2+} , the C2B domain tilts so that its CBLs immerse into PM, and consequentially the C2A domain detaches from Cpx, opening the Ca^{2+}-binding pocket (Fig. 9 (4)). Subsequent chelation of Ca^{2+} ions by the C2A domain triggers a conformational transition, which leads to the pre-fusion state characterized by the tips of both C2 domains being immersed into PM (Fig. 9 (5)).

Our simulations also suggest that if this pathway is disrupted, the PM-Syt1-SNARE-Cpx complex can transition to the state (Fig. 9 (6)) with both C2 domains being attached to PM prior to the Ca^{2+} chelation. Although this conformational state allows Ca^{2+} binding for both domains, the coupling between the CBLs of the C2A and C2B domains counteracts their insertion into PM. Respectively, a "dead-end" state (Fig. 9 (7)) is formed, which has the C2 domains of Syt1 tightly attached to PM but not penetrating into it.

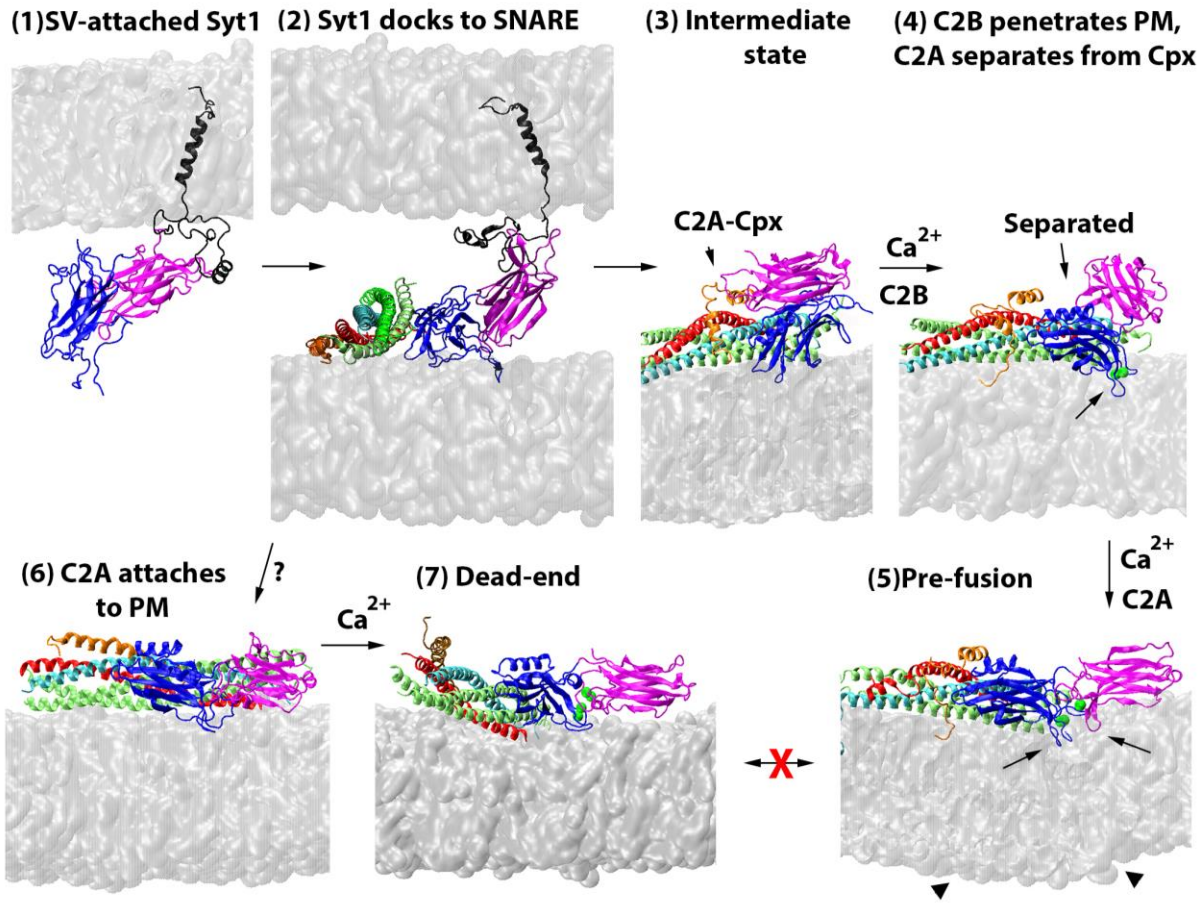

Fig. 9. The model of the dynamic formation of the prefusion complex. The SV-attached Syt1 (1) docks to the SNARE bundle and to PM via its C2B domain (2). Subsequently, an intermediate PM-Syt1-SNARE-Cpx complex (3) is formed via the attachment of the C2A domain to Cpx. Ca^{2+} chelation by the CBLs of the C2B domain (4) triggers the immersion of the C2B domain into PM followed by the separation of the C2A domain from Cpx (arrows). The subsequent Ca^{2+} chelation by the C2A domain leads to the pre-fusion state (5) which has the tips of both C2 domains penetrating into PM (arrows) and altering PM curvature (arrowheads). An alternative pathway may involve the attachment of the C2A domain to PM prior to the Ca^{2+} chelation (6), which would lead to the dead-end state upon Ca^{2+} binding (7), with the C2 domains of Syt1 being bridged and tightly attached to PM but not penetrating into the lipid bilayer.

Coordinated insertion of the tips of C2 domains of Syt1 into PM is a critical step in synaptic fusion, and it depends on the interactions of Syt1 with the SNARE complex

Biophysical studies of membrane fusion suggested that Syt1 triggers exocytosis via the insertion of the tips of its C2 domains into PM, locally promoting PM curvature, which in turn triggers

fusion[3, 9, 45] . A subsequent study demonstrated a direct correlation between membrane curvature and fusion, providing further evidence that Syt1-mediated membrane bending is a critical step in exocytosis[46]. Furthermore, optical studies demonstrated that the C2 domains of Syt1 act synergistically, interacting in the insertion into PM and membrane bending [47]. Thus, it is generally agreed that the synergistic coordinated insertion of the tips of the C2 domains Syt1 into PM is a critical step in synaptic fusion.

Syt1 interacts with the SNARE complex [48], and these interactions, largely mediated by SNAP25, are essential for exocytosis [15, 49, 50]. Monitoring exocytosis at PC12 cells demonstrated that Syt1 utilizes SNARE binding to promote the Ca^{2+}-dependent membrane bending and the fusion pore expansion [14]. Furthermore, our earlier MD study demonstrated that the interaction of Syt1 with the SNARE complex is required to uncouple the C2 domains of Syt1 and to promote their insertion into PM [2].

The present study shows that the coordinated insertion of the Ca^{2+}-bound tips of the C2 domains of Syt1 into PM depends on the sequence of Syt1 interactions and conformational transitions. We outline the conformational pathway that can leads to the formation of the pre-fusion PM-$4Ca^{2+}$Syt1-SNARE-Cpx complex, as well as an alternative pathway that could potentially inhibit fusion.

The Syt1-SNARE-Cpx complex can adopt multiple conformational states enroute to triggering fusion

The Syt1-SNARE complex was shown to adopt multiple conformational states *in vitro* [1, 18, 30-32] being structurally heterogenous. This raises the question of the structure and dynamics of this complex *in vivo*, between the lipid bilayers of SV and PM. The interactions of the C2 domains of Syt1 with lipids depend

on the lipid composition[51] and in particular on the PM component PIP_2 [52, 53]. Therefore, the proximity to PM could define the structure of the Syt1-SNARE complex.

A crystallography study [18] identified a large primary interface between the $\beta_1\beta_2$ $\beta_5\beta_8$ surface of the C2B and the t-SNARE bundle. Our subsequent MD study[2] relied on this data to build the all-atom model of the PM-4Ca^{2+}Syt1-SNARE-Cpx pre-fusion complex. Multiple lines of evidence suggest that this complex is formed *in vivo* and that its formation is required for the evoked synaptic transmission. First, this structure proved stable at a microsecond scale at physiological ion concentrations. Second, the intragenic screen in *Drosophila*[17] identified several Syt1 loss-of-function mutations, which involved the residues of the C2B domain that maintained the C2B-SNARE interactions**.** Third, our MD simulations[2] showed that the formation of this complex promotes the immersion of both C2 domains of Syt1 into PM, generating PM curvature and distortion. Finally, this simulations also showed that this complex drives merging of lipid bilayers mimicking PM and SV [2].

Here, we investigated the dynamic formation of the pre-fusion protein-lipid complex and found that the ability of the C2 domains to insert into PM upon Ca^{2+} binding depends on the conformational pathway. In particular, we identified a "dead-end" state of the complex, which does not allow the insertion of the tips of the C2 domains into PM due to the coupling between the CBLs of the C2 domains (Fig. 9 (7)). We also identified the sequence of the conformational transitions enabling the formation of the prefusion complex (Fig. 9, 2-5), starting from the docking of the C2B domain to SNAP25 and PM, proceeding via the formation of an intermediate complex mediated by the direct Syt1-Cpx attachment, undergoing a two stage Ca^{2+} chelation, and finally inserting the tips of C2 domains into PM. These findings suggest that the structural heterogeneity of the Syt1-SNARE complex observed *in vitro* reflects the dynamic flexibility of this complex required for its *in vivo* function.

Cpx may accelerate evoked release by promoting the intermediate state that leads to the formation of the pre-fusion protein-lipid complex

Our MD simulations unraveled the conformational pathway (Fig. 9, 2-5) that requires a direct role of Cpx in transitioning to the intermediate conformational state of the protein-lipid complex (Fig. 9 (3)). Cpx was shown to ubiquitously promote Ca^{2+}-dependent evoked transmission[24] and also to clamp spontaneous or asynchronous activity at several preparations[54], with these two Cpx functions being uncoupled [21, 55-57]. Although the Cpx clamping function is largely understood, being mediated by its accessory helix [55-58], the molecular mechanisms of the Cpx facilitatory action in evoked release are still debated[24, 54, 59, 60]. However, structural[30, 32], genetic[25] and functional[27, 28] studies suggest that Cpx may regulate evoked release by directly binding Syt1.

Our MD simulations led to the all-atom model of the intermediate PM-Syt1-SNARE-Cpx complex (Fig. 9 (3)) which has the C2A domain of Syt1 directly binding Cpx. Within this complex, the CBLs of the C2A domain attach to the region of Cpx that connects its central and accessory helixes, forming a salt bridge supported by strong hydrophobic interactions. Notably the Syt1-binding region of Cpx is positioned in the vicinity of the switch-breaker mutation [57] which was shown to selectively inhibit evoked transmission. The observed Syt1-Cpx attachment affects both proteins by 1) displacing the accessory helix of Cpx from the SNARE bundle, which could diminish the Cpx clamping function[55, 58], and 2) blocking the Ca^{2+} binding pocket of the C2A domain of Syt1. The latter mechanism enables Cpx to orchestrate the sequential Ca^{2+} chelation by the C2B and C2A domains and to prevent the formation of a dead-end state of the PM-Syt1-SNARE-Cpx complex.

A conformational switch defines the pattern of Ca^{2+} chelation by Syt1

In is generally agreed that Ca^{2+} triggers evoked release by binding Syt1 after an SV becomes docked to PM in the vicinity of Ca^{2+} channels[11, 12]. Indeed, the affinity of Syt1 to Ca^{2+} is relatively low, however it increases remarkably in the presence of phospholipids and especially PIP_2 [43, 61, 62]. Therefore, a cooperative action of Ca^{2+} and PIP_2 has been proposed[63]. In line with these studies, our MD simulations suggest that the C2B module chelates Ca^{2+} being already attached to PIP_2 via its PB stretch (Fig. 9 (3)).

Notably, the simulations also show that Ca^{2+} binding should take place prior to the attachment of the C2A module to PM, since otherwise the C2 domains can bridge their CBLs, which counteracts their insertion into PM (Fig. 9 (6)). We show that a fast Cpx-dependent conformational switch can orchestrate the subsequent Ca^{2+} chelation by the C2B domain and then by the C2A domain, preventing the "dead-end" scenario. This conformational switch acts at a sub-microsecond scale and releases the Cpx block from the C2A domain upon Ca^{2+} chelation by the C2B domain (Fig. 9, 3->4). This model agrees with earlier studies suggesting that the C2 domains of Syt1 are not equivalent in triggering fusion, and that the C2B domain has the primary role [64-66].

Promoting the dead-end state could inhibit fusion

Although the "dead-end" state of the PM-4Ca^{2+}Syt1-SNARE-Cpx complex (Fig. 9 (7)) was identified by the MD simulations, it remains to be investigated whether this state is adopted *in vivo*. Since we found that the Syt1-Cpx interactions are needed for the complex to transition into the pre-fusion state, it is likely that the complex could transition intto its dead-end state in the absence of Cpx. This may account for the reduced and desynchronized evoked release in the Cpx knockout preparations [20, 23, 25, 56].

Unfortunately, the time-scale of MD simulations is limited by microseconds, and therefore it does not allow us to evaluate the stability of the dead-end state of the PM-4Ca^{2+}Syt1-SNARE-Cpx complex. However, the multiple ionic interactions maintaining the complex, including the salt bridges linking the C2 domains to PIP_2 , as well as Ca^{2+} coordination bonds bridging the CBLs of the C2 domains, suggest that this state may be relatively stable. In this case, any mutations in Syt1 that favor the dead-end state could become dominant-negative, since the accumulation of the dead-end complexes could block the available release sites and preclude native Syt1 forms from docking to t-SNARE clusters and PIP_2-rich membrane patches. Notably, it was demonstrated that neutralizing Asp residues of the CBLs of the C2B domain produces the dominant negative phenotype in *Drosophila* [17, 64]. Furthermore, several disease-associated missense mutations in the CBLs of the C2B domain have been discovered, all causing

developmental neuropathies as heterozygotes [67-69]. Hypothetically, these mutations could alter the attachment of the CBLs of the C2B domain to PM[70], thus bypassing the intermediate complex (Fig. 9 (3)) and driving the transition into the dead-end state (Fig. 9, (6,7)). Further modeling and experimentation will be needed to test this hypothesis.

Methods

System setup

All the molecular systems were constructed using Visual Molecular Dynamics Software (VMD, Theoretical and Computational Biophysics Group, NIH Center for Macromolecular Modeling and Bioinformatics, at the Beckman Institute, University of Illinois at Urbana-Champaign). All the simulations were performed in water/ion environment with explicit water molecules. Potassium and chloride ions were added to neutralize the systems and to yield 150 mM concentration of KCl.

The lipid bilayer was constructed as described in [2].The phosphatidylcholine (POPC) lipid bilayers were generated using VMD. To mimic PM, the anionic lipid patch containing POPC, phosphatidylserine (POPS) and PIP_2 (75:20:5) was used. The initial structure of the POPC:POPS:PIP_2 bilayer [71] was kindly provided by Dr. J. Wereszczynski (Illinois Institute of Technology). We used the bilayer with one leaflet containing only POPC monomers, and the other leaflet having the POPC:POPS:PIP_2 (75:20:5) composition. The leaflets were merged manually using VMD and then optimized and equilibrated in water/ion environment. This approach ensured that the periodic image of the lipid bilayer mimicking PM served to mimic the neutral lipids composing SV. In all the systems, the lipid bilayers were positioned in the XY plain.

To build the model of full length Syt1^{fl} we employed the SWISS-MODEL server [72, 73].The sequence of human Syt1 (GeneBank: KAI2567145.1), excluding its luminal domain (residues 1-55) was used [74], and the structure of the C2AB tandem of Syt1[44] served as a template for generating the 3D structure of Syt1^{fl} .

The models of SNARE-Cpx complexes on PM were taken from earlier MD simulations [2]

Molecular dynamics

The MD simulations were performed employing CHARMM36 force field [75] modified to include the parameters for PIP_2 as described in [71]. The simulations were performed with periodic boundary conditions and Ewald electrostatics in NPT ensemble at 310K.

The heating (20 ps) and equilibration (100 ns) phases were performed employing NAMD [76] Scalable Molecular Dynamics (Theoretical and Computational Biophysics Group, NIH Center for Macromolecular Modeling and Bioinformatics, at the Beckman Institute, University of Illinois at Urbana-Champaign) through ACCESS (Advanced Cyberinfrastructure Coordination Ecosystem: Service and Support) at Stampede (TACC) and Anvil (Purdue) clusters. The NAMD simulations were performed with a flexible cell and with a time-step of 1.5 fs, employing Langevin thermostat and Berendsen barostate.

Production runs were performed at Anton2 supercomputer [36, 37] with Desmond software through the MMBioS (National Center for Multiscale Modeling of Biological Systems, Pittsburgh Supercomputing Center and D.E. Shaw Research Institute). All the Anton2 simulations were performed in a semi-isotropic regime, with a time-step of 2.5 fs, and employing the multigrator [77] to maintain constant temperature and pressure.

Analysis and Visualization

The trajectory analysis was performed employing VMD. All the parameters along all the trajectories were computed with a time step of 2.4 ns. The number of VdW contacts between two molecules was computed as the number of atomic pairs separated by less than 3 Å. The penetration of a protein into the lipid bilayer was computed as $p = Z_{lipid}^{max} - Z_{protein}^{min}$, where Z_{lipid}^{max} is the maximal atomic Z coordinate of the lipid bilayer, and $Z_{protein}^{min}$ is the minimal atomic Z coordinate of the protein [2]. The distributions of the parameters along MD trajectories were compared using the Kolomogorov-Smirnov (K.-S.) test.

Acknowledgements

Anton 2 computer time was provided by the Pittsburgh Supercomputing Center (PSC) through Grant R01GM116961 from the National Institutes of Health. The Anton 2 machine at PSC was generously made available by D.E. Shaw Research.

This work used Anvil and Stampede supercomputers through allocation from the Advanced Cyberinfrastructure Coordination Ecosystem: Services & Support (ACCESS) program, which is supported by National Science Foundation grants #2138259, #2138286, #2138307, #2137603, and #2138296.

Data availability

All simulations performed on Anton are available for distribution. The Database is maintained by the Pittsburgh Supercomputing Center (PSC). All the Anton users are required to provide a detailed description of their data for the PSC Database upon completion of a publication. In addition, all the structure and trajectory files are available from the author.

References

1. Zhou Q, Lai Y, Bacaj T, Zhao M, Lyubimov AY, Uervirojnangkoorn M, Zeldin OB, Brewster AS, Sauter NK, Cohen AE, et al. Architecture of the synaptotagmin-SNARE machinery for neuronal exocytosis. *Nature* 2015, 525:62-67.
2. Bykhovskaia M. SNARE complex alters the interactions of the Ca(2+) sensor synaptotagmin 1 with lipid bilayers. *Biophys J* 2021, 120:642-661.
3. Chapman ER. How does synaptotagmin trigger neurotransmitter release? *Annu Rev Biochem* 2008, 77:615-641.
4. Leitz J, Kavalali ET. Ca2+ Dependence of Synaptic Vesicle Endocytosis. *Neuroscientist* 2015.
5. Perin MS, Brose N, Jahn R, Sudhof TC. Domain structure of synaptotagmin (p65). *J. Biol. Chem* 1991, 266:623-629.
6. Ubach J, Zhang X, Shao X, Sudhof TC, Rizo J. Ca2+ binding to synaptotagmin: how many Ca2+ ions bind to the tip of a C2-domain? *EMBO J* 1998, 17:3921-3930.
7. Fernandez-Chacon R, Konigstorfer A, Gerber SH, Garcia J, Matos MF, Stevens CF, Brose N, Rizo J, Rosenmund C, Sudhof TC. Synaptotagmin I functions as a calcium regulator of release probability. *Nature* 2001, 410:41-49.
8. Nyenhuis SB, Karandikar N, Kiessling V, Kreutzberger AJB, Thapa A, Liang B, Tamm LK, Cafiso DS. Conserved arginine residues in synaptotagmin 1 regulate fusion pore expansion through membrane contact. *Nat Commun* 2021, 12:761.
9. Martens S, Kozlov MM, McMahon HT. How synaptotagmin promotes membrane fusion. *Science* 2007, 316:1205-1208.
10. Sudhof TC, Rothman JE. Membrane fusion: grappling with SNARE and SM proteins. *Science* 2009, 323:474-477.
11. Sudhof TC. Neurotransmitter release: the last millisecond in the life of a synaptic vesicle. *Neuron* 2013, 80:675-690.
12. Kaeser PS, Regehr WG. Molecular mechanisms for synchronous, asynchronous, and spontaneous neurotransmitter release. *Annu Rev Physiol* 2014, 76:333-363.
13. Rizo J, Xu J. The Synaptic Vesicle Release Machinery. *Annu Rev Biophys* 2015, 44:339-367.
14. Lynch KL, Gerona RR, Kielar DM, Martens S, McMahon HT, Martin TF. Synaptotagmin-1 utilizes membrane bending and SNARE binding to drive fusion pore expansion. *Mol Biol Cell* 2008, 19:5093-5103.
15. Schupp M, Malsam J, Ruiter M, Scheutzow A, Wierda KD, Sollner TH, Sorensen JB. Interactions Between SNAP-25 and Synaptotagmin-1 Are Involved in Vesicle Priming, Clamping Spontaneous and Stimulating Evoked Neurotransmission. *J Neurosci* 2016, 36:11865-11880.
16. Pang ZP, Shin OH, Meyer AC, Rosenmund C, Sudhof TC. A gain-of-function mutation in synaptotagmin-1 reveals a critical role of Ca2+-dependent soluble N-ethylmaleimide-sensitive factor attachment protein receptor complex binding in synaptic exocytosis. *J Neurosci* 2006, 26:12556-12565.
17. Guan Z, Bykhovskaia M, Jorquera RA, Sutton RB, Akbergenova Y, Littleton JT. A synaptotagmin suppressor screen indicates SNARE binding controls the timing and Ca(2+) cooperativity of vesicle fusion. *Elife* 2017, 6.

18. Brewer KD, Bacaj T, Cavalli A, Camilloni C, Swarbrick JD, Liu J, Zhou A, Zhou P, Barlow N, Xu J, et al. Dynamic binding mode of a Synaptotagmin-1-SNARE complex in solution. *Nat Struct Mol Biol* 2015, 22:555-564.
19. Chen X, Tomchick DR, Kovrigin E, Arac D, Machius M, Sudhof TC, Rizo J. Three-dimensional structure of the complexin/SNARE complex. *Neuron* 2002, 33:397-409.
20. Reim K, Mansour M, Varoqueaux F, McMahon HT, Sudhof TC, Brose N, Rosenmund C. Complexins regulate a late step in Ca2+-dependent neurotransmitter release. *Cell* 2001, 104:71-81.
21. Xue M, Lin YQ, Pan H, Reim K, Deng H, Bellen HJ, Rosenmund C. Tilting the balance between facilitatory and inhibitory functions of mammalian and Drosophila Complexins orchestrates synaptic vesicle exocytosis. *Neuron* 2009, 64:367-380.
22. Chang S, Reim K, Pedersen M, Neher E, Brose N, Taschenberger H. Complexin stabilizes newly primed synaptic vesicles and prevents their premature fusion at the mouse calyx of held synapse. *J Neurosci* 2015, 35:8272-8290.
23. Huntwork S, Littleton JT. A complexin fusion clamp regulates spontaneous neurotransmitter release and synaptic growth. *Nature Neuroscience* 2007, 10:1235-1237.
24. Trimbuch T, Rosenmund C. Should I stop or should I go? The role of complexin in neurotransmitter release. *Nat Rev Neurosci* 2016, 17:118-125.
25. Jorquera RA, Huntwork-Rodriguez S, Akbergenova Y, Cho RW, Littleton JT. Complexin controls spontaneous and evoked neurotransmitter release by regulating the timing and properties of synaptotagmin activity. *J Neurosci* 2012, 32:18234-18245.
26. Dhara M, Yarzagaray A, Schwarz Y, Dutta S, Grabner C, Moghadam PK, Bost A, Schirra C, Rettig J, Reim K, et al. Complexin synchronizes primed vesicle exocytosis and regulates fusion pore dynamics. *J Cell Biol* 2014, 204:1123-1140.
27. Xu J, Brewer KD, Perez-Castillejos R, Rizo J. Subtle Interplay between synaptotagmin and complexin binding to the SNARE complex. *J Mol Biol* 2013, 425:3461-3475.
28. Tang J, Maximov A, Shin OH, Dai H, Rizo J, Sudhof TC. A complexin/synaptotagmin 1 switch controls fast synaptic vesicle exocytosis. *Cell* 2006, 126:1175-1187.
29. Cao P, Yang X, Sudhof TC. Complexin activates exocytosis of distinct secretory vesicles controlled by different synaptotagmins. *J Neurosci* 2013, 33:1714-1727.
30. Zhou Q, Zhou P, Wang AL, Wu D, Zhao M, Sudhof TC, Brunger AT. The primed SNARE-complexin-synaptotagmin complex for neuronal exocytosis. *Nature* 2017, 548:420-425.
31. Lai AL, Huang H, Herrick DZ, Epp N, Cafiso DS. Synaptotagmin 1 and SNAREs form a complex that is structurally heterogeneous. *J. Mol. Biol* 2011, 405:696-706.
32. Brunger AT, Leitz J. The Core Complex of the Ca(2+)-Triggered Presynaptic Fusion Machinery. *J Mol Biol* 2023, 435:167853.
33. Rizo J, Sari L, Qi Y, Im W, Lin MM. All-atom molecular dynamics simulations of Synaptotagmin-SNARE-complexin complexes bridging a vesicle and a flat lipid bilayer. *Elife* 2022, 11.
34. Prasad R, Zhou HX. Membrane Association and Functional Mechanism of Synaptotagmin-1 in Triggering Vesicle Fusion. *Biophys J* 2020, 119:1255-1265.
35. Bykhovskaia M. Calcium binding promotes conformational flexibility of the neuronal Ca(2+) sensor synaptotagmin. *Biophys J* 2015, 108:2507-2520.
36. Shaw DE, Dror RO, Grossman JP, J.A. M, Bank JA, Young C, Deneroff MM, K.J. B, Chow E, Eastwood MP, et al. Millisecond-Scale Molecular Dynamics Simulations on

Anton. *Proceedings of the Conference on High Performance Computing, Networking, Storage and Analysis* 2009. Vol. SC09.
37. Shaw DE. Long molecular dynamics simulations of proteins: Progress, promise, and problems. *Abstracts of Papers of the American Chemical Society* 2014, 247.
38. Zanetti-Domingues LC, Korovesis D, Needham SR, Tynan CJ, Sagawa S, Roberts SK, Kuzmanic A, Ortiz-Zapater E, Jain P, Roovers RC, et al. The architecture of EGFR's basal complexes reveals autoinhibition mechanisms in dimers and oligomers. *Nat Commun* 2018, 9:4325.
39. Pan AC, Jacobson D, Yatsenko K, Sritharan D, Weinreich TM, Shaw DE. Atomic-level characterization of protein-protein association. *Proc Natl Acad Sci U S A* 2019, 116:4244-4249.
40. Voleti R, Jaczynska K, Rizo J. Ca(2+)-dependent release of synaptotagmin-1 from the SNARE complex on phosphatidylinositol 4,5-bisphosphate-containing membranes. *Elife* 2020, 9.
41. Wu Z, Ma L, Courtney NA, Zhu J, Landajuela A, Zhang Y, Chapman ER, Karatekin E. Polybasic Patches in Both C2 Domains of Synaptotagmin-1 Are Required for Evoked Neurotransmitter Release. *J Neurosci* 2022, 42:5816-5829.
42. Fernandez I, Arac D, Ubach J, Gerber SH, Shin O, Gao Y, Anderson RG, Sudhof TC, Rizo J. Three-dimensional structure of the synaptotagmin 1 C2B-domain: synaptotagmin 1 as a phospholipid binding machine. *Neuron* 2001, 32:1057-1069.
43. Radhakrishnan A, Stein A, Jahn R, Fasshauer D. The Ca2+ affinity of synaptotagmin 1 is markedly increased by a specific interaction of its C2B domain with phosphatidylinositol 4,5-bisphosphate. *J. Biol. Chem* 2009, 284:25749-25760.
44. Fuson KL, Montes M, Robert JJ, Sutton RB. Structure of human synaptotagmin 1 C2AB in the absence of Ca2+ reveals a novel domain association. *Biochemistry* 2007, 46:13041-13048.
45. Chernomordik LV, Kozlov MM. Mechanics of membrane fusion. *Nat Struct Mol Biol* 2008, 15:675-683.
46. Hui E, Johnson CP, Yao J, Dunning FM, Chapman ER. Synaptotagmin-mediated bending of the target membrane is a critical step in Ca(2+)-regulated fusion. *Cell* 2009, 138:709-721.
47. Liu H, Bai H, Xue R, Takahashi H, Edwardson JM, Chapman ER. Linker mutations reveal the complexity of synaptotagmin 1 action during synaptic transmission. *Nat Neurosci* 2014, 17:670-677.
48. Davis AF, Bai J, Fasshauer D, Wolowick MJ, Lewis JL, Chapman ER. Kinetics of synaptotagmin responses to Ca2+ and assembly with the core SNARE complex onto membranes. *Neuron* 1999, 24:363-376.
49. Gerona RR, Larsen EC, Kowalchyk JA, Martin TF. The C terminus of SNAP25 is essential for Ca(2+)-dependent binding of synaptotagmin to SNARE complexes. *J Biol Chem* 2000, 275:6328-6336.
50. Zhang X, Kim-Miller MJ, Fukuda M, Kowalchyk JA, Martin TF. Ca2+-dependent synaptotagmin binding to SNAP-25 is essential for Ca2+-triggered exocytosis. *Neuron* 2002, 34:599-611.
51. Davletov BA, Sudhof TC. A single C2 domain from synaptotagmin I is sufficient for high affinity Ca2+/phospholipid binding. *J Biol Chem* 1993, 268:26386-26390.

52. Bai J, Tucker WC, Chapman ER. PIP2 increases the speed of response of synaptotagmin and steers its membrane-penetration activity toward the plasma membrane. *Nat Struct Mol Biol* 2004, 11:36-44.
53. Bradberry MM, Bao H, Lou X, Chapman ER. Phosphatidylinositol 4,5-bisphosphate drives Ca(2+)-independent membrane penetration by the tandem C2 domain proteins synaptotagmin-1 and Doc2beta. *J Biol Chem* 2019, 294:10942-10953.
54. Mohrmann R, Dhara M, Bruns D. Complexins: small but capable. *Cell Mol Life Sci* 2015, 72:4221-4235.
55. Brady J, Vasin A, Bykhovskaia M. The Accessory Helix of Complexin Stabilizes a Partially Unzippered State of the SNARE Complex and Mediates the Complexin Clamping Function In Vivo. *eNeuro* 2021, 8.
56. Xue M, Reim K, Chen X, Chao HT, Deng H, Rizo J, Brose N, Rosenmund C. Distinct domains of complexin I differentially regulate neurotransmitter release. *Nat Struct Mol Biol* 2007, 14:949-958.
57. Cho RW, Kummel D, Li F, Baguley SW, Coleman J, Rothman JE, Littleton JT. Genetic analysis of the Complexin trans-clamping model for cross-linking SNARE complexes in vivo. *Proc Natl Acad Sci U S A* 2014, 111:10317-10322.
58. Radoff DT, Dong Y, Snead D, Bai J, Eliezer D, Dittman JS. The accessory helix of complexin functions by stabilizing central helix secondary structure. *Elife* 2014, 3.
59. Krishnakumar SS, Radoff DT, Kummel D, Giraudo CG, Li F, Khandan L, Baguley SW, Coleman J, Reinisch KM, Pincet F, et al. A conformational switch in complexin is required for synaptotagmin to trigger synaptic fusion. *Nat Struct Mol Biol* 2011, 18:934-940.
60. Ramakrishnan S, Bera M, Coleman J, Rothman JE, Krishnakumar SS. Synergistic roles of Synaptotagmin-1 and complexin in calcium-regulated neuronal exocytosis. *Elife* 2020, 9.
61. Lawrence SAS, Kirschbaum C, Bennett JL, Lutomski CA, El-Baba TJ, Robinson CV. Phospholipids Differentially Regulate Ca(2+) Binding to Synaptotagmin-1. *ACS Chem Biol* 2024.
62. Li L, Shin OH, Rhee JS, Arac D, Rah JC, Rizo J, Sudhof T, Rosenmund C. Phosphatidylinositol phosphates as co-activators of Ca2+ binding to C2 domains of synaptotagmin 1. *J Biol Chem* 2006, 281:15845-15852.
63. Kobbersmed JRL, Berns MMM, Ditlevsen S, Sorensen JB, Walter AM. Allosteric stabilization of calcium and phosphoinositide dual binding engages several synaptotagmins in fast exocytosis. *Elife* 2022, 11.
64. Lee J, Guan Z, Akbergenova Y, Littleton JT. Genetic analysis of synaptotagmin C2 domain specificity in regulating spontaneous and evoked neurotransmitter release. *J Neurosci* 2013, 33:187-200.
65. Gruget C, Bello O, Coleman J, Krishnakumar SS, Perez E, Rothman JE, Pincet F, Donaldson SH, Jr. Synaptotagmin-1 membrane binding is driven by the C2B domain and assisted cooperatively by the C2A domain. *Sci Rep* 2020, 10:18011.
66. Mackler JM, Drummond JA, Loewen CA, Robinson IM, Reist NE. The C(2)B Ca(2+)-binding motif of synaptotagmin is required for synaptic transmission in vivo. *Nature* 2002, 418:340-344.
67. Herrmann DN, Horvath R, Sowden JE, Gonzalez M, Sanchez-Mejias A, Guan Z, Whittaker RG, Almodovar JL, Lane M, Bansagi B, et al. Synaptotagmin 2 mutations

cause an autosomal-dominant form of lambert-eaton myasthenic syndrome and nonprogressive motor neuropathy. *Am J Hum Genet* 2014, 95:332-339.
68. Whittaker RG, Herrmann DN, Bansagi B, Hasan BA, Lofra RM, Logigian EL, Sowden JE, Almodovar JL, Littleton JT, Zuchner S, et al. Electrophysiologic features of SYT2 mutations causing a treatable neuromuscular syndrome. *Neurology* 2015, 85:1964-1971.
69. Baker K, Gordon SL, Melland H, Bumbak F, Scott DJ, Jiang TJ, Owen D, Turner BJ, Boyd SG, Rossi M, et al. SYT1-associated neurodevelopmental disorder: a case series. *Brain* 2018, 141:2576-2591.
70. Bradberry MM, Courtney NA, Dominguez MJ, Lofquist SM, Knox AT, Sutton RB, Chapman ER. Molecular Basis for Synaptotagmin-1-Associated Neurodevelopmental Disorder. *Neuron* 2020, 107:52-64 e57.
71. Alwarawrah M, Wereszczynski J. Investigation of the Effect of Bilayer Composition on PKCalpha-C2 Domain Docking Using Molecular Dynamics Simulations. *J Phys Chem B* 2017, 121:78-88.
72. Studer G, Tauriello G, Bienert S, Biasini M, Johner N, Schwede T. ProMod3-A versatile homology modelling toolbox. *PLoS Comput Biol* 2021, 17:e1008667.
73. Waterhouse A, Bertoni M, Bienert S, Studer G, Tauriello G, Gumienny R, Heer FT, de Beer TAP, Rempfer C, Bordoli L, et al. SWISS-MODEL: homology modelling of protein structures and complexes. *Nucleic Acids Res* 2018, 46:W296-W303.
74. Zimin AV, Shumate A, Shinder I, Heinz J, Puiu D, Pertea M, Salzberg SL. A reference-quality, fully annotated genome from a Puerto Rican individual. *Genetics* 2022, 220.
75. Vanommeslaeghe K, Hatcher E, Acharya C, Kundu S, Zhong S, Shim J, Darian E, Guvench O, Lopes P, Vorobyov I, et al. CHARMM general force field: A force field for drug-like molecules compatible with the CHARMM all-atom additive biological force fields. *J Comput Chem* 2010, 31:671-690.
76. Phillips JC, Braun R, Wang W, Gumbart J, Tajkhorshid E, Villa E, Chipot C, Skeel RD, Kale L, Schulten K. Scalable molecular dynamics with NAMD. *J. Comput. Chem* 2005, 26:1781-1802.
77. Lippert RA, Predescu C, Ierardi DJ, Mackenzie KM, Eastwood MP, Dror RO, Shaw DE. Accurate and efficient integration for molecular dynamics simulations at constant temperature and pressure. *J Chem Phys* 2013, 139:164106.